The Tempering of Iron-Carbon Martensite; Dilatometric and Calorimetric Analysis

LIU CHENG, C. M. BRAKMAN, B. M. KOREVAAR, and E. J. MITTEMEIJER

The aging behavior of iron-carbon martensite (1.13 wt pct C) between −190 °C and 450 °C was investigated by quantitative analysis of the corresponding changes in volume and enthalpy. A method to determine activation energies of the occurring solid-state transformations by performing nonisothermal measurements of some physical property of the specimen has been described. Martensitic specimens were prepared by carburizing pure iron and quenching in brine and liquid nitrogen. The dilatometric and calorimetric experiments were supplemented with microhardness measurements. At least five different stages of structural change can be distinguished, which are quantitatively analyzed in terms of their effects on volume and enthalpy: (i) transformation of retained austenite into martensite (between −180 and −100 °C); (ii) redistribution of carbon atoms (below 100 °C); (iii) precipitation of transition carbide (between 80 and 200 °C); (iv) decomposition of retained austenite (between 240 and 320 °C); and (v) conversion of transition carbide into cementite (between 260 and 350 °C).

I. INTRODUCTION: STAGES OF TEMPERING

THE tempering of iron-carbon martensite has been the subject of intensive investigation for more than 50 years. Although significant advances have been made in unraveling the processes underlying the tempering behavior, a complete and satisfactory understanding of the mechanisms of the structural changes involved has not yet been obtained.[1–4] According to the present state of knowledge the structural evolution of iron-carbon martensite on tempering can be divided into the following sequence of processes:

(a) Aging at and slightly above room temperature; a redistribution of the carbon atoms takes place, which is ascribed to:
(i) A segregation of carbon atoms to lattice defects.
(ii) The formation of clusters of carbon atoms in the iron matrix.
(b) The first stage of tempering, in the temperature range of about 80 to 180 °C,* involves the precipitation of a transition carbide (ε/η carbide) leaving a ferrite matrix containing the segregated carbon atoms (also described as low-carbon martensite).
(c) The second stage of tempering, temperature range about 200 to 300 °C, caused by the decomposition of retained austenite into ferrite and cementite.
(d) The third stage of tempering, temperature range about 250 to 350 °C, involves the conversion of the transition carbide and segregated carbon atoms into cementite.

*The temperature ranges of the different stages of tempering depend on the heating rates during the tempering process (here taken about 10 °C/min).

A wide range of experimental techniques has been applied to investigate the structural changes of martensite during tempering, including X-ray diffraction,[2,3,5,6] electron microscopy and diffraction,[7,8] resistometry,[1] and atom probe field ion microscopy.[9,10,11] However, not much attention has been given in the last decades to the analysis of volume and enthalpy changes. Also in view of recent instrumental and methodological developments of dilatometric and calorimetric techniques for the analysis of solid state transformations, a corresponding investigation of the tempering of iron-carbon martensite appears justified.[12,13]

In this paper results of an investigation of the tempering processes of pure iron-carbon martensite (1.1 wt pct C) are reported. Dilatometry, differential thermal analysis (DTA), and differential scanning calorimetry (DSC) were applied, in particular. It will be shown that the combination of dilatometry and calorimetry is very useful because of their complementary nature: tempering processes can be accompanied with a large heat production and a small change of length, and *vice versa*.

II. THEORETICAL BACKGROUND FOR KINETIC ANALYSIS

A. *Annealing with Constant Heating Rate*

Evaluation of kinetic reaction parameters such as activation energies can be performed by tracing the change in physical properties that reflect the course of the solid state transformation. The properties considered here are the specific volume (length, dilatometry) and the enthalpy (calorimetry).

The fraction transformed, f, can be defined as:

$$f = \frac{p - p_0}{p_1 - p_0} \qquad [1]$$

where p indicates the physical property measured and p_0 and p_1 denote the initial and final states before and after the transformation. Note that in a nonisothermal annealing experiment not only p, but also p_0 and p_1 can depend on the temperature.

Under isothermal conditions a heterogeneous solid-state transformation can often be described by the Johnson-Mehl-Avrami (JMA) equation:

LIU CHENG, Graduate Student, C. M. BRAKMAN, Senior Scientist, and B. M. KOREVAAR and E. J. MITTEMEIJER, Professors, are with the Laboratory of Metallurgy, Delft University of Technology, Rotterdamseweg 137, 2628 AL Delft, The Netherlands.

Manuscript submitted September 23, 1987.

$$f = 1 - \exp[-\beta^n] \qquad [2]$$

where $\beta = kt = k_0 t \exp[-E/RT]$, E is the effective activation energy, k_0 is a constant, n is the JMA exponent, and R, T, and t have the usual meaning. Application of the JMA equation in the case of *nonisothermal* annealing is not straightforward (for discussion see Reference 12).

For nonisothermal annealing with a constant heating rate, Φ, the following formula can be derived:[12,13]

$$\beta = \frac{T^2}{\Phi} \cdot \frac{R}{E} \cdot k\left\{1 - 2\left(\frac{RT}{E}\right) + \ldots\right\} \qquad [3]$$

where $\beta = \int_0^t k\,dt$. (Note that T and thus k depends on t; Eq. [3] is more generally valid than for JMA kinetics alone.[13]) The factor $2(RT/E)$ is usually $\ll 1$ and can be neglected.

On the basis of Eqs. [1], [2], and [3] a relation between the physical property p and the kinetic parameters E, n, and k_0 can be obtained.

B. *Temperature of Inflection Point*

An easily accessible experimental quantity is the temperature T_i corresponding to the inflection point of the p-$T(T \propto t)$ curve.

It has been shown that[12]

$$\ln \frac{T_i^2}{\Phi} = \frac{E}{RT_i} + \ln \frac{E}{Rk_0} + \text{Res. 1} + \text{Res. 2} \qquad [4]$$

where:

$$\text{Res. 1} = \left(\frac{2\left(\frac{dp_1}{dT} - \frac{dp_0}{dT}\right)}{p_1 - p_0}\right)_{T_i} \left(\frac{RT_i^2}{n^2 E}\right)$$

$$\text{Res. 2} = 2\left\{1 - \frac{1}{n^2} + n \ln\left[\frac{T_i^2}{\Phi} \frac{Rk(T_i)}{E}\right]\right\} \frac{RT_i}{E}$$

If both residuals (Res. 1 and Res. 2) can be neglected, the activation energy E can be derived from the slope of the straight line obtained by plotting $\ln T_i^2/\Phi$ *vs* $1/T_i$ for different values of Φ.

If p denotes length change, as recorded by the dilatometer, dp/dT equals the product of the length and the coefficient of expansion. Normally only minor differences occur between the expansion coefficients before and after the transformations considered and Res. 1 can be neglected. If p denotes enthalpy, dp/dT represents the heat capacity (measured directly in differential scanning calorimetry, DSC, or indirectly in differential thermal analysis, DTA). The differences in heat capacity before and after transformation are usually small, so Res. 1 can be neglected. Neglect of Res. 2 is nearly always justified.[12]

C. *Temperature of a Fixed Stage of Transformation*

If the heating rate is varied in a series of experiments, it follows, with reference to the discussion below Eq. [2], that in each heating experiment the parameter β will have the same value for a chosen fixed value for the stage of transformation f. Defining $T_{f'}$ as the temperature corresponding to that fixed value of f, f', and realizing that $RT_{f'}/E \ll 1$, it follows from Eq. [3] that

$$\ln \frac{T_{f'}^2}{\Phi} = \frac{E}{RT_{f'}} + \text{constant} \qquad [5]$$

and the activation energy E can be derived from the slope of the straight line obtained by plotting $\ln T_{f'}^2/\Phi$ *vs* $1/T_{f'}$.

Realizing that p or dp/dT rather than f or df/dT represents the signal recorded, it should be noted that the temperature dependence of the reference states p_0 and p_1 introduces uncertainties in the determination of $T_{f'}$ (*cf.* Eq. [1]). In fact, this statement parallels the recognition that the temperature of the inflection point T_i of the p curve does not coincide in general with the temperature of the inflection point of the f-curve; this led to the emergence of the residual terms in Eq. [4]. An analogous error analysis can be made for $T_{f'}$. In particular for the initial and final stages of the transformation the determination of $T_{f'}$ is not very accurate. Moreover, the importance of such temperature-dependent residual terms to be inserted into Eq. [5] can be relatively large in comparison with those in Eq. [4]. Therefore it is concluded that the determination of the activation energy by the method based on T_i is more accurate than by the method based on $T_{f'}$. However, the latter method may be fruitfully applied if the first method cannot be used (see later) or in the case that a possible change of the activation energy during the transformation should be analyzed.[13]

III. EXPERIMENTAL PROCEDURES

A. *Specimen Preparation*

The specimens were prepared from pure iron (0.0042 at. pct Ni; 0.009 at. pct Cu; 0.0014 at. pct Mn; <0.01 at. pct Si; 0.011 at. pct C; 0.001 at. pct N, balance Fe).

The material was cold rolled to a thickness of about 0.2 mm and recrystallized at 700 °C. From this sheet material cylindrical specimens were made by rolling up sheet material for the dilatometric experiments with a height of about 10 mm and a diameter of about 6.5 mm. For the DTA- and DSC experiments flat discs were prepared with a diameter of about 5 mm. The specimens were thoroughly cleaned in a solution of 50 pct HCl in ethanol to remove the oxide layer, polished, and slightly etched in 2 pct nital before carburizing.

The carburizing was performed in a vertical tube furnace at 842 °C for 2.5 hours in a gas stream (linear flowrate about 20 cm/min) consisting of 99.1 vol pct H_2 (Hoek-Loos; 99.995 vol pct) and 0.9 vol pct CO (Hoek-Loos: 99.5 vol pct). After carburizing the specimens were quenched in brine (10 wt pct NaCl in water) at room temperature.

The carbon content was determined by weighing the specimens before and after carburizing. The carbon content of the specimen was also determined by chemical analysis. Within the experimental accuracy data from the weight measurements agreed with those from chemical analysis. Further, the homogeneity of the carbon content within the specimens was checked by electron probe microanalysis and microhardness measurements performed on cross-sections of some specimens. Results are given in Figures 1 and 2. A practically homogeneous carbon distribution is obtained in a plate-martensite structure. The average carbon content of the carburized specimens, as determined by

Fig. 1—Optical micrograph (composite) of cross-section of carburized specimen quenched in brine. Etching reagent: 0.5 pct Nital.

chemical analysis, was 1.13 wt pct (±0.06 wt pct); this corresponds with an M_s temperature of about 180 °C.

Some of the specimens quenched in brine (code: BQ) were analyzed as such; the remainder of the specimens were further quenched in liquid nitrogen (code: BQ-LNQ) before being submitted to dilatometric or calorimetric experiments.

B. *Isothermal Aging; Hardness Measurements*

Specimens (BQ-LNQ) were aged at room temperature for up to one month and at 60 °C for up to 225 hours. Further, specimens (BQ-LNQ) were tempered for 1 hour at constant temperatures between room temperature and 450 °C (in argon gas to prevent oxidation and decarburization). The microhardness (Leitz Durimet instrument; 300 g load) was determined as a function of aging time and temperature. Each hardness value is the average of at least ten measurements (results are given in Figures 3 and 4).

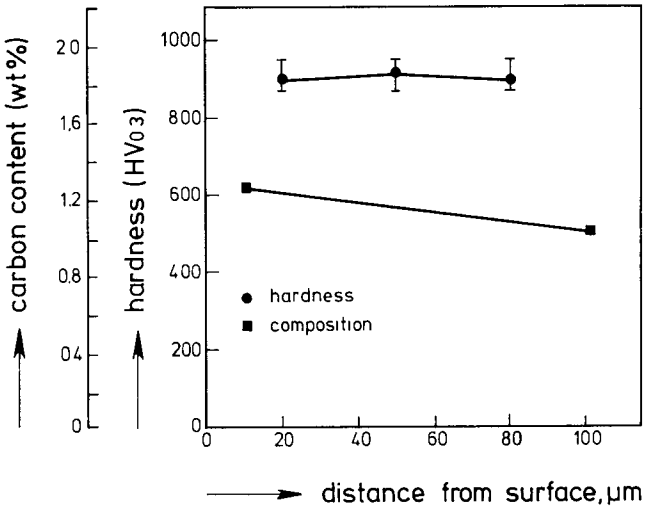

Fig. 2—Microhardness and carbon distribution (electron probe microanalysis) across the cross-section of a carburized and brine quenched specimen.

C. *Annealing with Constant Heating Rate*

1. *Dilatometry*

Dilatometric analysis was performed using a Dupont Thermomechanical Analyser, type 942. For a number of constant heating rates the length change and its derivative with respect to time were registered applying a Dupont Thermal Analyser type 1090. Specimens treated in various ways were subjected to subsequent dilatometric analysis:

(i) Quenched in brine, mounted in the dilatometer, and subsequently quenched in liquid nitrogen (BQ-LNQ). The time at room temperature necessary for inserting the specimen in the dilatometer was about 5 minutes (Figure 5).
(ii) Quenched in brine, and mounted in the dilatometer (BQ) (Figure 6).
(iii) Quenched in brine, aged at room temperature for various times before being mounted in the dilatometer, and subsequently quenched in liquid nitrogen (BQ-x hours RT-LNQ; x = 0.1 to 96 hours) (Figure 5).
(iv) Quenched in brine, mounted in the dilatometer, and quenched in liquid nitrogen, thereafter aged at room temperature for various times and again quenched in liquid nitrogen (BQ-LNQ-x hours RT-LNQ) (Figure 7).

After these treatments the specimens were heated from −196 °C to 500 °C or from room temperature to 500 °C (BQ specimens) applying (constant) heating rates in the range 5 to 40 °C/min.

For the quantitative analysis given in this paper it is assumed that the volume changes of the specimen are isotropic.

2. *Calorimetry*

Two different instruments were used: a Stanton-Redcroft apparatus (type DTA 671) and a Perkin-Elmer DSC apparatus (type 2). The experiments were performed in a protective gas atmosphere of 90 vol pct Ar and 10 vol pct H_2 to prevent oxidation and decarburization. Specimens treated in various ways were subjected to subsequent calorimetric analysis:

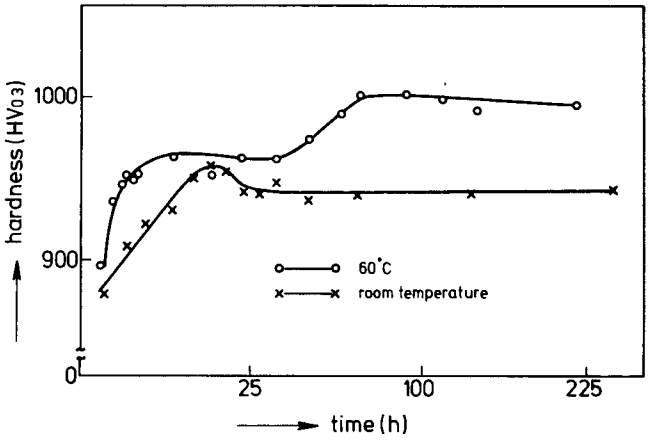

Fig. 3—Hardness of BQ-LNQ specimens as a function of aging time at room temperature and at 60 °C.

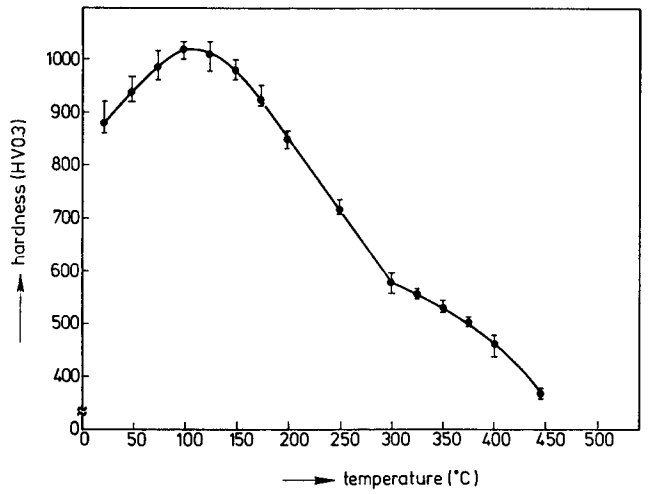

Fig. 4—Hardness of BQ-LNQ specimens as a function of tempering temperature. Each specimen was tempered for 1 h at the indicated temperatures.

(i) BQ-LNQ (Figure 8).
(ii) BQ-LNQ-x hours RT; x = 0.5 to 720 hours (Figure 9).
(iii) BQ-LNQ-1 hour 150 °C (Figure 10).
(iv) BQ-1 hour 150 °C (Figure 11).

After these treatments the specimens were inserted in the DTA apparatus which was subsequently filled with protective gas and cooled to −70 °C by liquid nitrogen.

Nonisothermal annealing (from −70 °C to 450 °C) occurred employing heating rates in the range 10 to 30 °C/min. After reaching 450 °C the apparatus was rapidly cooled to −70 °C. In order to determine the base line the experiment was repeated under the same conditions with the now tempered specimen. The bulk of the experiments was performed in the DTA apparatus; a number of supplementary experiments were done in the DSC apparatus (protective gas: argon) which gave better reproducibility, but for DSC analysis the specimens could not be cooled below room temperature.

D. *Retained Austenite*

The amount of retained austenite in the specimens was determined by X-ray diffraction analysis.[14] In the BQ-LNQ specimens 6 vol pct and in the BQ specimens 15 vol pct of retained austenite was found.

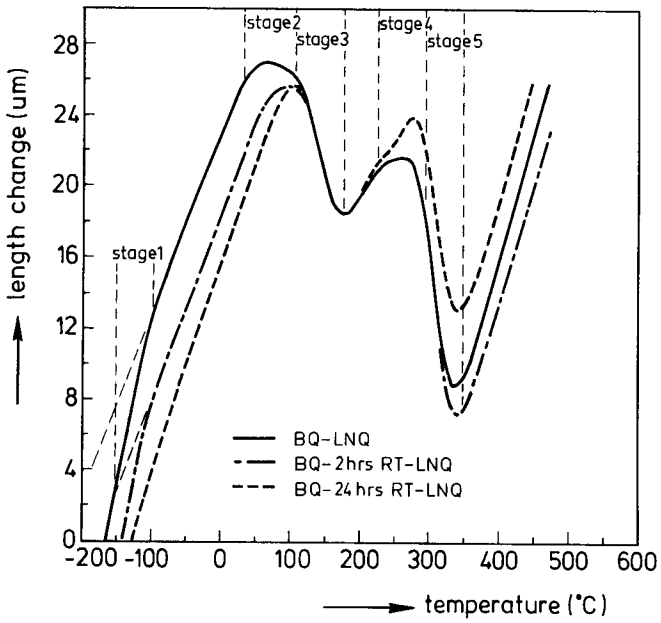

Fig. 5—Dilatometer curves for BQ-x hours RT-LNQ specimens aged at room temperature for 0.1 h, 2 h, and 24 h (initial length about 10.5 mm, heating rate 10 °C/min).

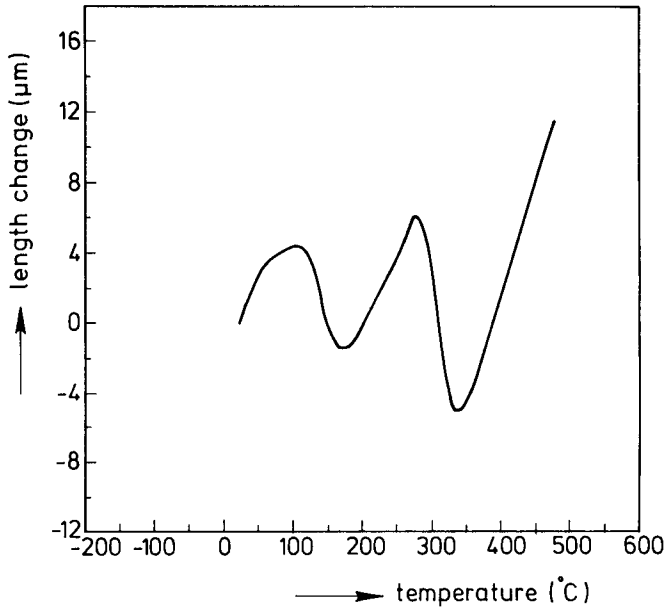

Fig. 6—Dilatometer curve for a BQ specimen. Initial length 10.44 mm; heating rate 10 °C/min.

IV. INCREASE OF SPECIFIC VOLUME BETWEEN −180 AND −100 °C: MARTENSITIC TRANSFORMATION OF RETAINED AUSTENITE

From the results of dilatometric and calorimetric experiments, examples of which are given in Figures 5 through 11, different stages of structural change can be distinguished. An effect of the first stage was found only by dilatometry. Between −180 and −100 °C an "abnormal" length increase occurred; see Figure 5. The average value

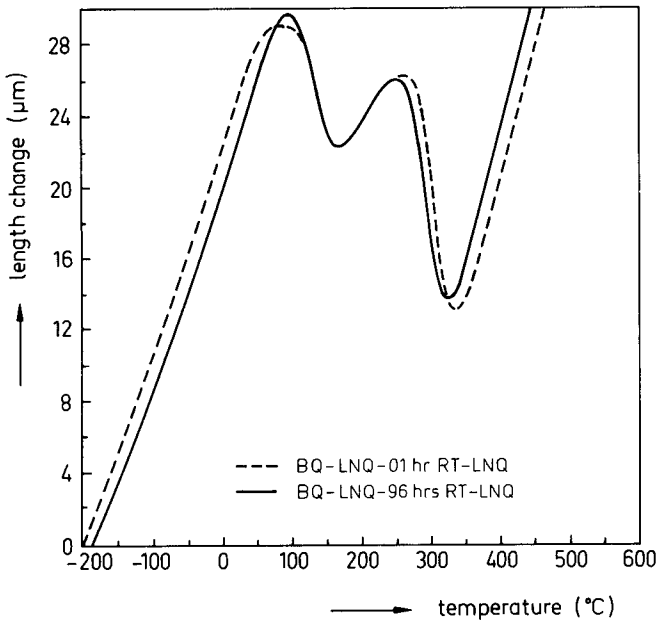

Fig. 7—Dilatometer curves for a BQ-LNQ-0.1 h R*T*-LNQ specimen (initial length 10.17 mm; heating rate 10 °C/min) and for a BQ-LNQ-96 h R*T*-LNQ specimen (initial length 10.72 mm, heating rate 5 °C/min).

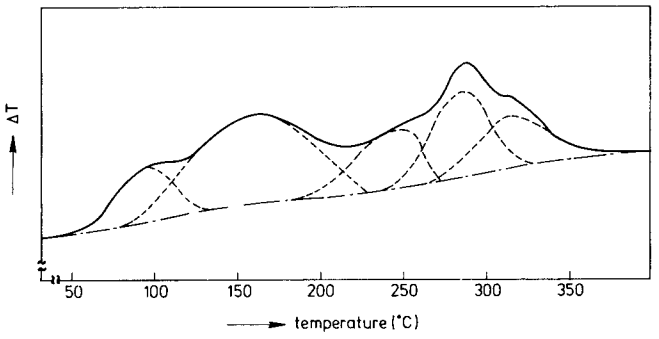

Fig. 8—DTA curve for a BQ-LNQ specimen. Heating rate 20 °C/min (ΔT = temperature difference between specimen and reference).

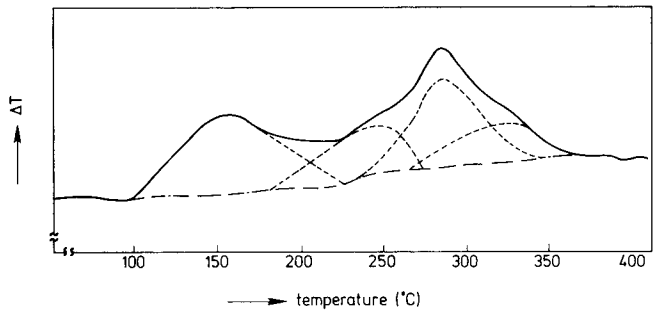

Fig. 9—DTA curve for a BQ-LNQ-168 h R*T* specimen. Heating rate 20 °C/min.

of this length increase was 0.053 pct. This change of specific volume of the specimens was observed for the BQ-LNQ-specimens; for the BQ-LNQ-*x* hours R*T*-LNQ specimens the effect was absent (*cf.* Figure 7). Aging of the BQ specimens at room temperature for long times, before cooling in liquid nitrogen, also suppressed the effect, whereas after a short aging time the effect was still observed; *cf.* Figure 5.

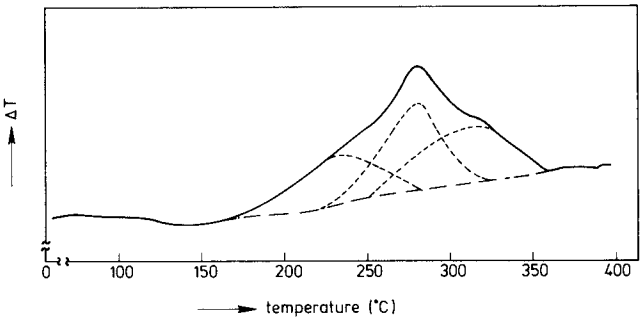

Fig. 10—DTA curve for a BQ-LNQ-1 h 150 °C specimen. Heating rate 20 °C/min.

To the authors' knowledge this peculiar increase of specimen volume of martensitic iron-carbon alloys has not been reported before in the literature, although comparable effects have been found in Fe-Ni-alloys.[15] The corresponding structure change has not been further investigated here, but the following explanation is offered. At the temperature concerned the atomic mobility is too small for any long range diffusion of, for example, carbon atoms. Therefore it is suggested that a martensitic transformation of (a part of) the retained austenite is responsible for the increase in specific volume. According to literature data, given in Table I, the difference in specific volume between austenite and martensite containing 1.1 wt pct C is about 4 pct. So the volume increase found in the BQ-LNQ specimens of about 0.16 pct indicates a transformation of about 4 pct of retained austenite during heating up to room temperature.

The above explanation is supported by the following additional observations.

An effect on length of retained austenite decomposition at temperatures between 250 °C and 300 °C (stage 4) has been observed for the BQ-24 hours RT-LNQ specimen (Figure 5), which is larger than that for the BQ-2 hours RT-LNQ specimen (Figure 5; see Section VII); it is well known that aging at room temperature causes a stabilization of the retained austenite. Further, an increase in magnetic saturation measured between −180 and −100 °C has been observed,[16] which also hints at transformation of retained austenite into martensite.

V. PREPRECIPITATION STAGES: REDISTRIBUTION OF CARBON ATOMS ON AGING

Aging in the temperature range between about 0 and 80 °C leads to a redistribution of carbon atoms within the iron lattice. Two different preprecipitation processes are distinguished:

(i) Segregation of carbon atoms to lattice defects, as for example indicated by resistometry[17] and atom probe field ion microscopy.[9] The sites for carbon enrichment can be at dislocations and twin boundaries for low and high carbon martensites, respectively.

(ii) Clustering of carbon atoms within the matrix as for example indicated by Mössbauer spectroscopy,[18] electron- and X-ray-diffraction analysis,[6,7,8] and atom probe field ion microscopy.[9,10,11]

It seems likely that at most about 0.15 to 0.2 wt pct C can segregate.[17,19] Part or all of the segregation can occur

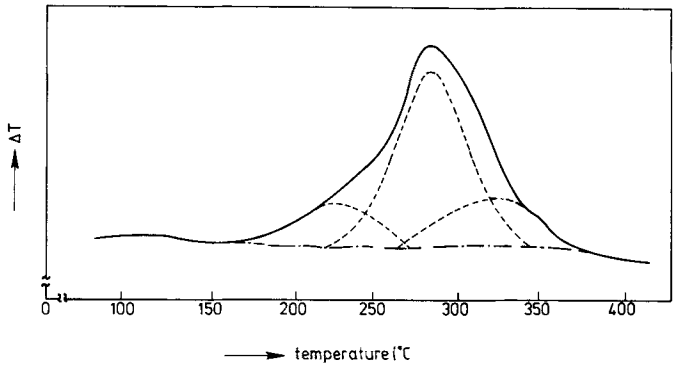

Fig. 11—DTA curve for a BQ-1 h 150 °C specimen. Heating rate 20 °C/min.

already during quenching if the M_s temperature is sufficiently high (so-called "auto tempering"). There are indications in the literature[20] that most of the segregation occurs within a few hours of aging at room temperature, if it has not been completed during quenching.

It will be shown below that the preprecipitation stages are accompanied by significant changes in hardness, specific volume, and enthalpy.

A. *Hardness*

The change of hardness on isothermal aging at 20 °C and at 60 °C is shown in Figure 3. The dependence of hardness on the tempering temperature is shown in Figure 4. Scatter of the measured data points is ascribed to the presence of regions of relatively soft retained austenite in the hard martensite. The hardness at room temperature first shows an increase of about 80 HV 0.3 (after 15 hours of aging); thereafter the hardness decreases somewhat (about 20 HV 0.3) in the next 20 hours and further remains constant within experimental accuracy. On aging at 60 °C the initial increase of the hardness was also found; a second increase of about 70 HV 0.3 is ascribed to the precipitation of the transition carbide (Section VI). In the specimens tempered for 1 hour at the temperatures indicated (Figure 4), the hardness increases up till 100 °C with about 150 HV 0.3.

The hardness change at room temperature is ascribed to the clustering process. Clustering leads to regions with low and high carbon contents. As a result, coherency strains in the lattice build up and consequently cause a hardness increase. At a later stage coarsening of the clusters could occur, as suggested in Reference 11, and this could explain the subsequent small hardness decrease. The hardness increase on nonisothermal tempering (Figure 4) can be explained as the combined effect of clustering at the lower temperatures and of precipitation at the higher temperatures.

B. *Specific Volume*

Apart from volume increase by thermal expansion, a decrease of specific volume/length is apparent in specimens which have not or only shortly been aged at room temperature for the temperature range 30 to 100 °C where a "flat maximum" occurs, in contrast with the "sharp maximum" observed in specimens which experienced extended aging at room temperature (compare the dilation curves given in Figures 5 and 7). Clearly, extended aging at room temperature before dilatometric analysis is responsible for this change of shape of the dilatometric curve.

Comparing the dilatation effects in specimens aged at room temperature for 0, 0.1, 2, 24, and 96 hours, respectively (Figures 5 and 7), it is concluded that more than half of the process responsible for the length decrease between 30 and 100 °C has taken place within 2 hours. It is unlikely that clustering of carbon atoms would lead to a change of specific volume since the carbon atoms remain dissolved in the iron matrix lattice (developing coherency strains due to clustering are expected to lead to displacements of iron atoms in the matrix such that a finite mean square displacement results but a negligible mean displacement occurs (see also Reference 3); hence, the average lattice parameter and thus volume are not affected). The decrease of volume is ascribed to segregation of interstitials to lattice defects: a loss of dissolved interstitials for the iron matrix implies a contraction, while initially empty sites (at dislocation cores, grain boundaries) become occupied. From Figures 5 and 7 it follows that the specific length change of marten-

Table I. Crystallographic Data

Phase	Structure	Lattice Parameters (Å)	Number Fe Atoms per Unit-Cell	Volume per Fe Atom (Å^3)	Source
Martensite	bct	$a = 2.8664 - 0.013$ wt pct C $c = 2.8664 + 0.116$ wt pct C	2	12.188 (1.1 wt pct C)	24
Ferrite	bcc	$a = 2.8664$	2	11.78	25
Austenite	fcc	$a = 3.555 + 0.044$ wt pct C	4	11.697 (1.1 wt pct C)	26
ε-carbide	hex.	$a = 2.752$ $c = 4.353$	2	14.275	27
ε-carbide	hex.	$a = 2.735$ $c = 4.335$	2	14.041	21
η-carbide	ortho-rhombic	$a = 4.704$; $b = 4.318$ $c = 2.830$	4	14.371	22
Cementite	ortho-rhombic	$a = 4.5234$; $b = 5.0883$ $c = 6.7426$	12	12.933	29

site during the aging process equals about 0.05 pct for pure martensite. If it is assumed that segregation implies the occupation by carbon atoms of initially empty sites leaving behind a matrix impoverished in carbon, the percentage of segregated carbon can be calculated from the dependence of the martensite-lattice parameters on carbon content (Table I). The experimentally determined volume change of 0.15 pct is then equivalent to 0.05 wt pct (0.23 at. pct) of segregated carbon. This value is considerably less than the value usually given in the literature for the total amount of segregated carbon (0.15 to 0.20 wt pct; see above), suggesting that a large part of the segregation takes place during cooling. (Note that the M_s temperature for the alloy considered is about 180 °C.)

C. *Enthalpy*

The DTA curve for the BQ-LNQ specimen (Figure 8) shows a pronounced heat effect between 40 and 100 °C, which is absent in the DTA curve for the specimen aged for 1 week at room temperature (Figure 9). Hence the redistribution of the carbon atoms during aging at room temperature is also associated with an appreciable production of heat. In the DTA/DSC curves this heat effect cannot be separated accurately from that corresponding to the precipitation of the transition carbides in the first stage of tempering, because serious overlapping occurs (see Figure 8 and Section VI). However, the latter effect will be independent of the aging treatment at room temperature, because the transition carbide does not precipitate at room temperature during the aging times employed (*e.g.*, see Reference 9 and Table I in Reference 13). After the carbon redistribution has been completed at room temperature its heat effect will be absent in the DTA/DSC curves obtained on subsequent nonisothermal annealing, while the effect of precipitation of the transition carbides remains (Figure 12). Thus the amount of heat generated (for preprecipitation + precipitation of transition carbide) decreases with aging time and reaches a constant value after about 70 hours. By extrapolating the total heat effect to zero aging time and subtracting the constant value for transition carbide precipitation, the heat produced by aging at room temperature was determined. After correction for retained austenite, a heat effect of about 240 J/mole martensite was obtained.

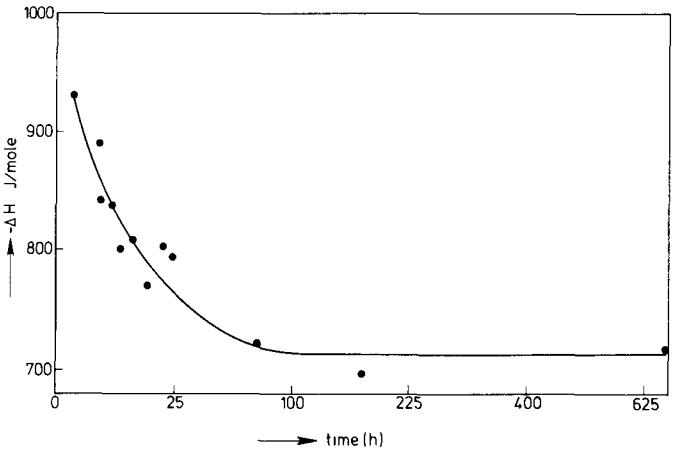

Fig. 12—Heat evolution ($-\Delta H$; in Joules per mole alloy BQ-LNQ) *vs* aging time at room temperature. $-\Delta H$ is the heat effect produced by the redistribution of carbon atoms and the precipitation of the transition carbides.

A comparison of the changes of length, hardness, and enthalpy produced on aging at room temperature shows an important difference: expressed as percentage of the total change due to preprecipitation, the change after two hours of aging is about 30 pct in heat effect and about 35 pct in hardness, whereas the change in length is about 60 pct (*cf.* Figures 5 and 7). This difference in time scale indicates that the mechanism dominating the length change is different from the mechanism governing the changes in enthalpy and hardness. Because the length change is caused by segregation of carbon atoms to dislocations and/or (twin) boundaries in the martensite (see above), it follows that the change in heat effect and hardness is *mainly* due to the clustering of the carbon atoms. (This does not imply that segregation is not accompanied by heat production; however, only a small amount of carbon atoms segregates in the present alloy on aging at room temperature; see above.)

D. *Kinetics*

For an investigation of the kinetics of the aging processes at room temperature, JMA analysis was first applied to the heat effect curve in Figure 12 (dominated by clustering, see above) as follows:

$$1 - f = \frac{-\Delta H_t - (-\Delta H_\infty)}{-\Delta H_0 - (-\Delta H_\infty)} = \exp - (kt)^n$$

where f is the fraction of the aging process passed through and $-\Delta H_t$, $-\Delta H_0$, and $-\Delta H_\infty$ denote the heat effects at times t, 0, and ∞, respectively (ΔH = reaction enthalpy).

Fitting the above equation to the experimental data leads to the results:

(a) relaxation time k^{-1} (at room temperature) = 10.3 hours (see also Table I in Reference 13);
(b) exponent n = 0.8.

Because of the overlap between the heat effects caused by aging and transition carbide-precipitation and the lack of a clear maximum in the heat-effect curves (Figure 8), the operating *activation energy for clustering* was determined by application of the method based on the temperature for a

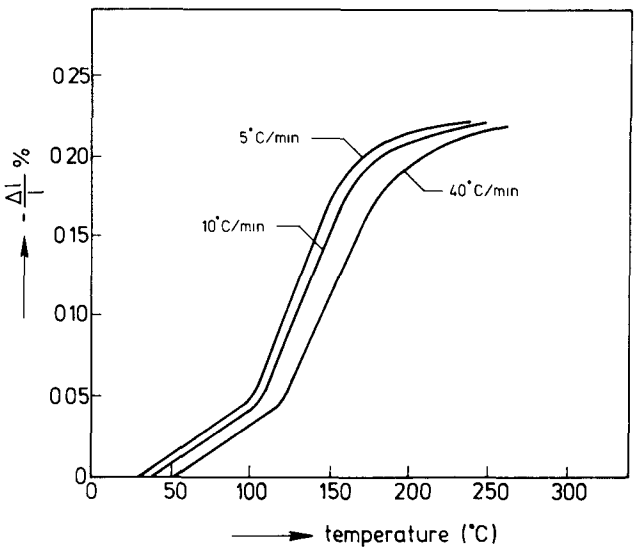

Fig. 13—Relative changes of length ($\Delta l/l$) caused by the redistribution of carbon atoms (below ±100 °C) and by the precipitation of transition carbides (100 °C to 200 °C).

fixed stage of the transformation (Eq. [5], Section II; $f' = 0.5$) to the results of DSC experiments for a number of heating rates:

$$E = 79 \text{ kJ/mole}$$

In Figure 13 the length change of some BQ/LNQ specimens, as caused by the segregation of carbon atoms (below 100 °C) and by the precipitation of transition carbides (100 to 250 °C), is given for various heating rates. Using the method based on a fixed stage of transformation ($f' = 0.5$) the operating *activation energy for segregation* was obtained as

$$E = 83 \text{ kJ/mole}$$

The activation energies obtained for the segregation and for the clustering of carbon atoms both point to the diffusion of carbon as the rate-controlling mechanism. However, the time scales of the processes are different. Segregation is more readily completed as only a limited number of sites are available for segregation. Clustering can start as a compositional modulation with a small amplitude, which can grow out after segregation has been finished.

VI. THE FIRST STAGE OF TEMPERING: PRECIPITATION OF THE TRANSITION CARBIDE

Tempering between about 80 °C and 200 °C leads to the precipitation of a transition carbide in the originally martensitic phase. The structure and composition of this carbide, designated as ε- or η-carbide, are not well known.[21,22,23] The segregated carbon atoms do not take part in this precipitation process.[17,19] The iron matrix after the first stage of tempering is denoted here as ferrite containing at most 0.15 to 0.20 wt pct of segregated carbon atoms (see Section V), instead of as "low carbon martensite".

A. *Hardness*

The precipitation of ε/η-carbide is associated with a maximum in the hardness around 100 °C, followed by a decrease on rising temperature (Figure 4). The maximal hardness is ascribed to the precipitation of a coherent carbide. The subsequent decrease of the hardness can be due to the reduction of the extent of the strain fields as a consequence of the coherent-incoherent transition of the carbides (about the same maximal hardness occurs on isothermal aging at 60 °C, Figure 3).

B. *Specific Volume*

A large decrease of specific volume/length occurs in the temperature range concerned (stage 3; Figures 5 through 7, 13). In the following a quantitative analysis of the length change is given.

A prediction of the length change induced by a solid-state transformation can be based on values reported in the literature for the lattice parameters of parent and product phases. Such lattice-parameter data normally hold at room temperature. Then, for comparison of the theoretically predicted length change at room temperature, T_r, with the experimental one taken at elevated temperature, T, a correction for the temperature difference should be made according to

$$\Delta l(T_r) = \Delta l(T) - [l_{fi}(T_r)\alpha_{fi} - l_{st}(T_r)\alpha_{st}]\Delta T \qquad [6]$$

where l and α are length and linear expansion coefficient of the specimen in either the untransformed (subscript *st*) or transformed (subscript *fi*) condition ($\Delta l = l_{fi} - l_{st}$; $\Delta T = T - T_r$).

Using literature data (Table II) the linear expansion coefficient, α_1, for the mixture of martensite and retained austenite was calculated as a volume weighted average for BQ-LNQ yielding:

$$\alpha_1 = 12.2 \cdot 10^{-6} \text{ (°C)}^{-1}$$

and analogously the linear expansion coefficient, α_2, for the mixture of ferrite (0.2 wt pct C), transition carbide and retained austenite was obtained as

$$\alpha_2 = 12.4 \cdot 10^{-6} \text{ (°C)}^{-1}$$

where the linear expansion coefficient of the transition carbide was taken equal to that of cementite.

For α_1 the calculated and experimentally determined values are in good agreement; α_2 cannot be determined experimentally because of the overlapping of the first and following stages of tempering.

After application of the described corrections (Eq. [6] with $\alpha_{st} = \alpha_1$ and $\alpha_{fi} = \alpha_2$), the average relative length change for the combined processes of preprecipitation and the first stage of tempering for pure martensite is obtained as:

$$\frac{\Delta l}{l} = -(0.23 \pm 0.03) \text{ pct}$$

from both BQ and BQ-LNQ specimens after correction for the amounts of retained austenite. Subtracting the estimated length effect for preprecipitation (−0.05 pct, Section V), yields a net relative length change for the first stage of tempering of:

$$\frac{\Delta l}{l} = -0.18 \text{ pct}$$

The crystallographic data for calculation of the volume effects are collected in Table I. The uncertain crystal structure and composition of the transition carbide and the variation in the lattice parameters reported in the literature lead to large differences in the calculated volume effects. The relative change of volume of the martensitic phase $\Delta V/V$ was calculated according to both:

(a) $$\alpha' \longrightarrow \alpha_s + \varepsilon\text{-Fe}_y\text{C}$$

$$\frac{\Delta V}{V} = \frac{\left(\frac{100 - (1+y)X + yX_s}{2}\right)v_{\alpha_s} + \frac{y}{2}(X - X_s)v_\varepsilon - \left(\frac{100 - X}{2}\right)v_{\alpha'}}{\left(\frac{100 - X}{2}\right)v_{\alpha'}}$$

and

(b) $$\alpha' \longrightarrow \alpha_s + \eta - \text{Fe}_y\text{C}$$

$$\frac{\Delta V}{V} = \frac{\left(\frac{100 - (1+y)X + yX_s}{2}\right)v_{\alpha_s} + \frac{y}{4}(X - X_s)v_\eta - \left(\frac{100 - X}{2}\right)v_{\alpha'}}{\left(\frac{100 - X}{2}\right)v_{\alpha'}}$$

Table II. Linear Thermal Expansion Coefficients[28]

Phase	Linear Expansion Coefficient (10^{-6} (°C)$^{-1}$)
Ferrite	14.5
Austenite	23.0
Martensite	11.5
Cementite	12.5

where α' denotes martensite, α_s indicates ferrite containing segregated carbon, X and X_s are the total carbon-atom percentage and the segregated carbon-atom percentage, respectively, the unit cell-volume of phase i is denoted by v_i, and y is the atom ratio of iron and carbon in the transition carbide. In Table III results of these calculations are given for $X = 5$ at. pct C ($\hat{=}$ 1.13 wt pct C) and for $X_s = 0$ (no segregation) and $X_s = 1$ at. pct C ($\cong$ 0.2 wt pct C) with values of $y = 2$, 2.5, and 3 and lattice parameters of α, α', ε-, and η-carbide given in Table I. The lattice parameter of α_s is taken equal to that of ferrite in agreement with results obtained in Reference 2.

According to Section V segregation does take place; then reasonable agreement between the experimental result ($\Delta V/V \cong 3\Delta l/l = -0.54$ pct; see above) and the calculated result is obtained for a composition of the transition carbide indicated as Fe_3C and for a segregation of 1 at. pct C (~0.2 wt pct C), using lattice-parameter data for the transition carbide from either Reference 22 or Reference 27. The lattice-parameter data for ε as given in Reference 21 appear to give less likely results (see Table III).

C. *Enthalpy*

The heat effect of the first stage of tempering can be deduced from Figure 12 as discussed in Section V. A heat release of 760 J/mole martensite is obtained for the precipitation of the transition carbide.

D. *Kinetics*

The activation energy for the precipitation of the transition carbide was determined from the change of the corresponding inflection-point temperatures in the dilatometric curves as a function of heating rate (*cf.* Eq. [4]):

$$E = 126 \text{ kJ/mole}.$$

It was verified that the residual terms in Eq. [4] could indeed be neglected. A value for this activation energy was also obtained by applying the same method to DSC curves:

$$E = 111 \text{ kJ/mole}$$

In a study devoted to the tempering of Fe-Ni-C-martensite, it has been proposed that iron diffusion along dislocations could be the rate determining step for the precipitation of ε/η-carbide.[1] According to Reference 30, the pipe diffusion of iron atoms is associated with an activation energy of 134 kJ/mole, to be compared with the values in the range of 111 to 126 kJ/mole reported above. Such dislocations can be generated to accommodate the volume misfit between transition carbide and matrix (about 17 pct for the Fe-C-alloy considered here).

VII. THE SECOND AND THIRD STAGES OF TEMPERING: DECOMPOSITION OF RETAINED AUSTENITE AND CONVERSION OF TRANSITION CARBIDE

At least two processes occur during tempering between about 200 °C and 360 °C: the decomposition of retained austenite into ferrite and cementite (second stage of tempering) and the conversion of transition carbide in cementite (third stage of tempering). The temperature ranges corresponding to these processes largely overlap and therefore an integrated discussion of the results obtained will be given. In particular for the second and third stages of tempering the combined application of dilatometry and calorimetry is very useful because the operating processes show opposite behavior: large change of specific volume is associated with small change of enthalpy and *vice versa*.

A. *Hardness*

After the precipitation of the ε/η-carbide in the first stage of tempering, a further increase of temperature initially leads to coarsening of the transition-carbide particles, with an associated decrease in the hardness (see Figure 4). At 300 °C a kink in the hardness curve indicates another change of the structure. Both the decomposition of retained austenite into ferrite and cementite and the conversion of transition carbide into initially fine cementite are expected

Table III. Calculated Volume Effects ($\Delta V/V$; in Pct) of the First Stage of Tempering for 5 At. Pct C ($\cong$ 1.1 Wt Pct C)

Transformation	$X_s = 0$ At. Pct	$X_s = 1$ At. Pct	v_ε or v_η (Å^3)
$\alpha' \rightarrow \alpha_s + \varepsilon\text{-}Fe_2C$	−1.19	−1.62	
$\alpha' \rightarrow \alpha_s + \varepsilon\text{-}Fe_{2.5}C$	−0.65	−1.19	28.550
$\alpha' \rightarrow \alpha_s + \varepsilon\text{-}Fe_3C$	−0.12	−0.76	(Ref. 27)
$\alpha' \rightarrow \alpha_s + \varepsilon\text{-}Fe_2C$	−1.39	−1.78	
$\alpha' \rightarrow \alpha_s + \varepsilon\text{-}Fe_{2.5}C$	−0.91	−1.39	28.082
$\alpha' \rightarrow \alpha_s + \varepsilon\text{-}Fe_3C$	−0.42	−1.0	(Ref. 21)
$\alpha' \rightarrow \alpha_s + \eta\text{-}Fe_2C$	−1.10	−1.56	
$\alpha' \rightarrow \alpha_s + \eta\text{-}Fe_{2.5}C$	−0.55	−1.11	57.484
$\alpha' \rightarrow \alpha_s + \eta\text{-}Fe_3C$	−0.00	−0.66	(Ref. 22)

to cause a relative increase in the hardness. However, the amount of retained austenite is small in the BQ-LNQ hardness specimens (Figure 4). Also the temperature range of the hardness increase agrees well with those of the changes in length and enthalpy associated with the cementite precipitation in the martensitic matrix (see below). So it is concluded that the retardation of the hardness decrease in Figure 4 is mainly due to the latter process.

B. *Specific Volume*

In the temperature range between 200 and 350 °C a large (relative) length reduction takes place (Figures 5 through 7). This length change is composed of the overlapping effects of the second and third stages of tempering which cannot be separated from each other. Therefore a direct comparison with theoretically predicted length (volume) changes cannot be made. However, an indirect quantitative approach is possible.

The *total* length change evoked by preprecipitation and the three stages of tempering is obtained from the experiments as:

$$\frac{\Delta l}{l} = -0.57 \text{ pct} \quad \text{for BQ-LNQ specimens}$$

$$\frac{\Delta l}{l} = -0.47 \text{ pct} \quad \text{for BQ specimens.}$$

These data hold at room temperature since corrections for temperature differences have been made in accordance with Eq. [6] (see Section VI; the calculated value for the linear expansion coefficient of the mixture of ferrite and cementite, $14.1 \cdot 10^{-6}$ $(°C)^{-1}$ (see Table II) agreed well with the average experimental value, $13.4 \cdot 10^{-6}$ $(°C)^{-1}$).

A theoretical prediction for the total relative change of volume is obtained from

(a) $$\alpha' \longrightarrow \alpha + \theta$$

$$\frac{\Delta V}{V} = \frac{\frac{100 - 4X}{2} v_\alpha + \frac{3X}{12} v_\theta - \frac{100 - X}{2} v_{\alpha'}}{\frac{100 - X}{2} v_{\alpha'}}$$

and:

(b) $$\gamma \longrightarrow \alpha + \theta$$

$$\frac{\Delta V}{V} = \frac{\frac{100 - 4X}{2} v_\alpha + \frac{3X}{12} v_\theta - \frac{100 - X}{4} v_\gamma}{\frac{100 - X}{4} v_\gamma}$$

where θ and γ denote cementite and (retained) austenite, respectively, and v_θ and v_γ are the volumes of the corresponding unit cells (for other symbols used, see Section VI). Using the crystallographic data gathered in Table I, the relative volume changes corresponding to the above reactions have been calculated for $X = 5$ at. pct C ($\cong$ 1.13 wt pct C) yielding:

$$\alpha' \longrightarrow \alpha + \theta: \quad \frac{\Delta V}{V} = -1.85 \text{ pct}$$

$$\gamma \longrightarrow \alpha + \theta: \quad \frac{\Delta V}{V} = +2.27 \text{ pct}$$

With the amounts of retained austenite of 6 pct in BQ-LNQ and 15 pct in BQ specimens (Section III), the following predictions for the total length change are thus obtained:

$$\frac{\Delta l}{l} = -0.54 \text{ pct} \quad \text{for BQ-LNQ specimen} \quad \text{and}$$

$$\frac{\Delta l}{l} = -0.41 \text{ pct} \quad \text{for BQ-specimens,}$$

in fair agreement with the experimental values given above.

Subtracting the experimental values for the length change of the preprecipitation stage and of the first stage of tempering (see Sections V and VI; corrected for retained austenite) from the calculated value for the total change of length gives the following length effects for the transformation of transition carbide into cementite:

$$\frac{\Delta l}{l} = -0.32 \text{ pct} \quad \text{for BQ-LNQ specimens} \quad \text{and}$$

$$\frac{\Delta l}{l} = -0.22 \text{ pct} \quad \text{for BQ-specimens.}$$

The significant *decrease* of length observed in Figures 5 through 7 between 260 °C and 350 °C is governed by this effect.

The decomposition of retained austenite leads to an *increase* of length of the specimen. This predicted increase amounts to

$$\frac{\Delta l}{l} = +0.045 \text{ pct} \quad \text{for BQ-LNQ specimens} \quad \text{and}$$

$$\frac{\Delta l}{l} = +0.11 \text{ pct} \quad \text{for BQ-specimens}$$

and takes place between 240 °C and 320 °C (see the following discussion of the enthalpy change). The reaction rate for the decomposition of austenite is maximal at about 285 °C, well below the corresponding temperature for the transformation of transition carbide (about 320 °C). As compared to Figure 5 (BQ-LNQ specimens: relatively small amount (6 vol pct) of retained austenite), in Figure 6 (BQ specimen: relatively large amount (15 vol pct) of retained austenite), a small anomaly in the length change is observed in the temperature range where the above-discussed decrease of length (as a result of the onset of transition-carbide transformation) becomes apparent. This is interpreted as caused by the decomposition of retained austenite.

Further, using the above reasoning, a comparison of the discussed parts of the dilatation curves of differently aged specimens (Figure 5) shows that, after brine quenching, an aging treatment of 24 hours at room temperature impedes the transformation of austenite into martensite on subsequent liquid nitrogen quenching, whereas 2 hours of aging at room temperature after brine quenching does not.

C. *Enthalpy*

A pronounced heat production occurs in the temperature range concerned: a peak with shoulders (long tails at the low- and high-temperature sides) is observed in the DTA scans (Figures 8 through 11). The temperature of the peak's maximum is well below 300 °C, indicating that the process

which dominates the change of enthalpy is different from that which governs the big length decrease occurring at higher temperatures (see above). It is concluded that the peak in heat production is evoked by the decomposition of retained austenite. The observation that this peak is much less pronounced for a BQ-LNQ specimen than for a BQ specimen (*cf.* Figures 10 and 11) is consistent with this interpretation. As a consequence, the shoulder at the high-temperature side (280 to 360 °C) is ascribed to the transformation of transition carbide into cementite. The shoulder at the low-temperature side (180 to 260 °C) is more difficult to interpret. It may be due to the precipitation of segregated carbon (see Section V) as cementite. However,

(i) The transition of segregated carbon to cementite is expected to cause a relative length increase, while in the indicated temperature range a small length decrease (0.04 pct) is found experimentally (Figures 5 through 7).
(ii) As the binding energy of carbon to dislocations is larger than in the transition carbide (*cf.* Section VI), the transformation of segregated carbon to cementite at a lower temperature than the transformation of the transition carbide into cementite is not likely.

An alternative explanation might be the formation of a second type of transition carbide, *e.g.*, Häggs or χ-carbide ($Fe_{2.5}C$). According to References 31 and 32 some χ-carbide is formed at martensite twin boundaries in this temperature range. A small length decrease as found in this region (see above) is predicted by calculation for a limited precipitation of this carbide.

The heat effects of the reactions discussed above overlap and cannot be accurately separated in a single calorimetric curve. Yet the heat generated by the decomposition of retained austenite can be obtained from specially devised experiments as follows.

It is assumed that the precipitation of transition carbide in a BQ and in a BQ-LNQ specimen tempered for 1 hour at 150 °C is complete (see Figures 10 and 11). Then, for these specimens the total heat produced on annealing, $-\Delta H_{tot}$, is the sum of those due to the reactions $\gamma \rightarrow \alpha + \theta$ and $\alpha_s + \varepsilon/\eta \rightarrow \alpha + \theta$, denoted as $-\Delta H_\gamma$ and $-\Delta H_{\alpha_s+\varepsilon/\eta}$, respectively:

$$\Delta H_{tot} = m\Delta H_\gamma + (1 - m)\Delta H_{\alpha_s+\varepsilon/\eta}$$

where m is the mole fraction of austenite. (Thus the change of enthalpy of the above-discussed process, corresponding with the shoulder at the low-temperature side of the DTA peak, is incorporated in $\Delta H_{\alpha_s+\varepsilon/\eta}$.) The two unknowns, ΔH_γ and $\Delta H_{\alpha_s+\varepsilon/\eta}$, can be determined if ΔH_{tot} is known for two values of m. From the results presented in Figures 10 and 11, are obtained: $-\Delta H_\gamma = 5$ kJ/mole austenite and $-\Delta H_{\alpha_s+\varepsilon/\eta} = 1$ kJ/mole martensite.

Combining the results on enthalpy changes reported in Sections V, VI, and above, it follows that the total heat produced on tempering one mole martensite containing 1.13 wt pct C equals

$$(0.24 + 0.76 + 1)\ \text{kJ} = 2\ \text{kJ}$$

D. *Kinetics*

The results reported above make evident that a value for the activation energy of the decomposition of retained austenite cannot be obtained by means of dilatometry but by use of calorimetry; the reverse holds for the transformation of transition carbide.

Using the method based on Eq. [4], by DSC analysis the following value for the activation energy of the decomposition of retained austenite was obtained:

$$E = 132\ \text{kJ/mole}$$

This value is approximately equal to the activation energy for the diffusion of C in γ-Fe: 128 kJ/mole, as obtained by graphical interpolation from Figure 9 in Reference 33.

Applying the same method in the dilatometric analysis leads to the following value for the activation energy of the transformation of the transition carbide:

$$E = 203\ \text{kJ/mole}$$

Analogous to the discussion devoted to the activation energy for the precipitation of transition carbide in the first stage of tempering (Section VI), significant rearrangement and transport of iron atoms is required on precipitation of cementite in the ferrite matrix obtained after the first stage of tempering (specific volume difference of about 10 pct, note that a one-to-one place correspondence of ε/η particle and θ particle is unlikely, because, in contrast with ε/η, θ nucleates preferentially at grain and twin boundaries of the tempered martensite[32]). Pipe diffusion along dislocations utilized for accommodation of this volume misfit can occur. However, as compared to the precipitation of transition carbides in the first stage of tempering, the higher temperatures involved in the precipitation of cementite in the third stage of tempering make the contribution of pipe diffusion to the overall transport of iron atoms less significant. Thus, the effective activation energy can be in the range indicated by the value for pipe diffusion of iron, 134 kJ/mole,[30] and the value for volume diffusion of iron, 251 kJ/mole[34] (*cf.* experimental value above).

VIII. CONCLUSIONS

At least five different stages of structural change are distinguished on tempering liquid nitrogen quenched iron-carbon martensite (1.13 wt pct C) between −195 and +450 °C (see also Table IV).

1. *Transformation of retained austenite into martensite between −180 and −100 °C.* The transformation causes an increase of length of the specimen of about 0.05 pct. The effect is suppressed by an aging treatment of 24 hours at room temperature.
2. *Redistribution of carbon atoms on aging below +100 °C.* Two processes are distinguished: segregation to dislocations and (twin) boundaries and clustering. Both processes are controlled by the volume diffusion of carbon (activation energies of about 80 kJ/mole). Carbon segregation induces a length decrease ($\Delta l/l \cong -0.05$ pct for pure martensite), whereas clustering of carbon atoms occurs without an apparent change of length. Clustering causes a hardness maximum on aging at room temperature (ΔHV ≅ 80 HV 0.3). The heat production observed (about 0.24 kJ/mole) is mainly due to clustering.

Table IV. Survey of Results

Process / Effect	1 Martensite Formation	2 Carbon Segregation and Clustering	3 Precipitation of Transition Carbide	4 Transform. of Retained Austenite	5 Precipitation of Cementite
Temperature range (°C)	−180-100	below 100	80-200	240-320	260-350
Volume change	+	−	− −	+	− −
Enthalpy change		+	+ +	+ +	+ +
Hardness change		+	+ → −		+
Rate-controlling mechanism	diffusion-less transformation	volume diffusion of carbon in martensite	pipe diffusion of iron atoms in ferrite	volume diffusion of carbon in austenite	pipe and volume diffusion of iron in ferrite
Activation energy (kJ/mole)		~80	~120	~130	~200

3. *Precipitation of transition carbide (ε/η) between 80 and 200 °C.* This process causes a further increase of hardness (ΔHV $\cong$ 70 HV 0.3), followed by a decrease; a large length decrease ($\Delta l/l \cong -0.18$ pct for pure martensite) and an appreciable evolution of heat ($\cong$ 0.76 kJ/mole martensite). The value found for the activation energy ($\cong$ 120 kJ/mole) suggests rate control by diffusion of iron atoms along dislocations for accommodation of the volume misfit between carbide and matrix.
4. *Decomposition of retained austenite between 240 and 320 °C.* This process causes a small length increase and a large evolution of heat ($\cong$ 5 kJ/mole austenite). The value found for the activation energy ($\simeq$ 130 kJ/mole) indicates volume diffusion of carbon in austenite as rate-controlling mechanism.
5. Conversion of *ε/η carbide into cementite between 260 and 350 °C.* This process is accompanied by a large length decrease ($\Delta l/l \cong -0.34$ pct for pure martensite) and a large evolution of heat ($\cong$ 1 kJ/mole martensite). The value found for the activation energy ($\simeq$ 200 kJ/mole) suggests that combined volume and pipe diffusion of iron is rate controlling.

ACKNOWLEDGMENTS

The authors are indebted to Mr. P. J. van der Schaaf for skillful experimental assistance, to Mr. A. H. L. M. Klijnhout for chemical analysis, to Ir. M. A. J. Somers for X-ray analysis, and to Ir. D. Schalkoord and Ing. E. J. A. van Dam for electron probe microanalysis.

REFERENCES

1. A. M. Sherman, G. T. Eldis, and M. Cohen: *Metall. Trans. A*, 1983, vol. 14A, pp. 995-1005.
2. P. C. Chen and P. G. Winchell: *Metall. Trans. A*, 1980, vol. 11A, pp. 1333-39.
3. P. C. Chen, B. O. Hall, and P. G. Winchell: *Metall. Trans. A*, 1980, vol. 11A, pp. 1323-31.
4. G. B. Olson and M. Cohen: *Metall. Trans. A*, 1983, vol. 14A, pp. 1057-65.
5. M. L. Bernshtein, L. M. Kaputkina, and S. D. Prokoshkin: *Scripta Metall.*, 1984, vol. 18, pp. 863-68.
6. H. Hayakawa, M. Tanigami, and M. Oka: *Metall. Trans. A*, 1985, vol. 16A, pp. 1745-50.
7. S. Nagakura, Y. Hirotsu, M. Kusunoki, T. Suzuki, and Y. Nakamura: *Metall. Trans. A*, 1983, vol. 14A, pp. 1025-31.
8. M. Kusunoki and S. Nagakura: *J. Appl. Cryst.*, 1981, vol. 14, pp. 329-36.
9. M. K. Miller, P. A. Beaven, and G. D. W. Smith: *Metall. Trans. A*, 1981, vol. 12A, pp. 1197-1204.
10. M. K. Miller, P. A. Beaven, S. S. Brenner, and G. D. W. Smith: *Metall. Trans. A*, 1983, vol. 14A, pp. 1021-24.
11. L. Chang and G. D. W. Smith: personal communication, Univ. of Oxford, 1987.
12. E. J. Mittemeijer, A. van Gent, and P. J. van der Schaaf: *Metall. Trans. A*, 1986, vol. 17A, pp. 1441-45.
13. E. J. Mittemeijer, Liu Cheng, P. J. van der Schaaf, C. M. Brakman, and B. M. Korevaar: *Metall. Trans. A*, 1988, vol. 19A, pp. 925-32.
14. C. F. Jatczak, J. A. Larson, and S. W. Shiu: *Retained Austenite and Its Measurement by X-Ray Diffraction*, SP 453, SAE Inc. Warrendale, PA, 1980.
15. C. A. V. de A. Rodrigues, C. Prioul, J. Plusquellec, and P. Y. Azou: *Proc. Int. Conf. on Solid Phase Transformations*. Carnegie-Mellon University, Pittsburgh, PA, 1981, pp. 1391-95.
16. I. Wierszyłowski: Technical University of Poznan, private communication, 1987.
17. G. R. Speich: *Trans. TMS-AIME*, 1969, vol. 245, pp. 2553-64.
18. W. K. Choo and R. Kaplow: *Acta Metall.*, 1973, vol. 21, pp. 725-32.
19. M. van Rooyen and E. J. Mittemeijer: *Scripta Metall.*, 1982, vol. 16, pp. 1255-60.
20. B. M. Mogutnov, V. M. Polovov, and L. A. Shvartsman: *Phys. Met. Metall.*, 1968, vol. 25, pp. 97-105.
21. K. H. Jack: *J.I.S.I.*, 1951, vol. 169, pp. 26-36.
22. Y. Hirotsu and S. Nagakura: *Acta Metall.*, 1972, vol. 20, pp. 645-55.
23. L. G. E. Hofer, E. M. Cahn, and W. C. Peebles: *J. Am. Chem. Soc.*, 1949, vol. 71, pp. 189-95.
24. P. G. Winchell and M. Cohen: *Trans. A.S.M.*, 1962, vol. 55, pp. 347-61.
25. R. C. Ruhl and M. Cohen: *Trans. AIME*, 1969, vol. 245, pp. 241-51.
26. C. S. Roberts: *Trans. AIME*, 1953, vol. 197, pp. 203-04.
27. S. Nagakura: *J. Phys. Soc. Japan*, 1959, vol. 14, pp. 186-95.
28. B. G. Lifshitz: *Physical Properties of Metals and Alloys*, Mashgiz, Moscow, 1956, p. 257.
29. Powder Diffraction File, A.S.T.M. card, 6-0688.
30. M. Cohen: *Trans. J.I M.*, 1970, vol. 11, pp. 145-51.
31. Y. Ohmori and S. Sugisawa: *Trans. J.I.M.*, 1971, vol. 12, pp. 170-78.
32. Y. Imai, T. Ogura, and A. Inoue: *Trans. I.S.I.J.*, 1973, vol. 13, pp. 183-91.
33. C. Wells, W. Batz, and R. F. Mehl: *Trans. AIME*, 1950, vol. 188, pp. 533-60.
34. F. S. Buffington, K. Hirano, and M. Cohen: *Acta Metall.*, 1961, vol. 9, pp. 434-39.